Frequency stabilization to 6×10^{-16} via spectral-hole burning

Michael J. Thorpe[1]*, Lars Rippe[2], Tara M. Fortier[1], Matthew S. Kirchner[1] and Till Rosenband[1]

We demonstrate two-stage laser stabilization based on a combination of Fabry–Pérot and spectral-hole burning techniques. The laser is first pre-stabilized by the Fabry–Pérot cavity to a fractional-frequency stability of $\sigma_y(\tau) < 1 \times 10^{-13}$. A pattern of multiple spectral holes written in the absorption spectrum of $Eu^{3+}:Y_2SiO_5$ serves to further stabilize the laser to $\sigma_y(\tau) \leq 6 \times 10^{-16}$ for $2\,s \leq \tau \leq 8\,s$. We also measure the frequency sensitivity of $Eu^{3+}:Y_2SiO_5$ spectral holes to environmental perturbations including temperature (16 kHz K^{-2}), pressure (211.4 Hz Pa^{-1}) and acceleration ($7 \times 10^{-12}\,g^{-1}$). Each spectral hole sensitivity parameter is lower than the corresponding parameter for Fabry–Pérot cavities, suggesting that spectral holes can be more frequency-stable.

Frequency-stable laser local oscillators (LLOs) are the limiting components of the new generation of optical atomic clocks. Quieter LLOs would allow optical clocks to run more stably, yielding faster comparisons, for more precise gravitational measurements and fundamental tests[1–3]. Quieter LLOs may also yield lower-phase-noise microwave oscillators by frequency division via femtosecond laser frequency combs[4–6].

State-of-the-art LLOs are based on lasers that are tightly locked to high-finesse Fabry–Pérot (FP) cavities constructed from low-thermal-expansion glass. The Pound–Drever–Hall (PDH) locking technique[7] provides sufficient signal-to-noise ratio (SNR) to lock the laser to the FP cavity, so that the frequency stability of the laser beyond $\tau = 0.1$ s is limited by the optical-length stability of the cavity. Over the past decade, stability has improved from 3×10^{-16} for durations of 1–100 s (ref. 8) to 2×10^{-16} for durations of 2–10 s (ref. 9). Practical concerns such as vibration sensitivity have been addressed[10–14], but lowering the noise floor has proved challenging. Numata and colleagues identified thermomechanical noise as the fundamental physical effect that limits the length stability of cavities[15], and this insight was confirmed experimentally[16]. Thermomechanical noise may be reduced by using longer cavities[9], by choosing cavity, mirror and mirror-coating materials with a reduced mechanical loss tangent, by operating the cavity at lower temperatures or by using larger-diameter optical modes. However, all of these approaches present significant technical difficulties due to the intrinsic sensitivity of FP cavities to changes in length.

Spectral-hole burning in cryogenically cooled crystals has been demonstrated as an alternative to FP cavities for laser stabilization[17–20]. In such systems, the instantaneous laser frequency is compared to the spectral memory stored as a narrow transparency in the absorption spectrum of the crystal, and an error signal is derived to stabilize the laser. A fractional-frequency stability of $\sigma_y(\tau = 10\,ms) = 3 \times 10^{-14}$ was demonstrated[18], but at longer times the instability was significantly higher due to the transient nature of holes in $Tm^{3+}:Y_2Al_5O_{12}$ and high photon fluxes that acted to degrade the spectral memory. Although initial demonstrations did not reach the stability of FP cavities, we expect the fundamental thermomechanical noise limit to be lower, because spectral holes are atomic frequency references that are perturbed only weakly through coupling to the crystal host. Hence, the

spectral-hole reference frequency is largely decoupled from the thermomechanical noise of the crystal.

Several properties of $Eu^{3+}:Y_2SiO_5$ have motivated high-resolution spectroscopy of spectral holes. Both the ground ($^7F_0$) and excited ($^5D_0$) states of the Eu^{3+} laser stabilization transition have small magnetic moments, making them insensitive to magnetic field fluctuations[21]. The $^5D_0$ excited state has a lifetime of 1.9 ms, and photon echo measurements indicate linewidths as low as 122 Hz for the $^7F_0 \rightarrow {}^5D_0$ transition[22,23]. When Eu^{3+} is doped
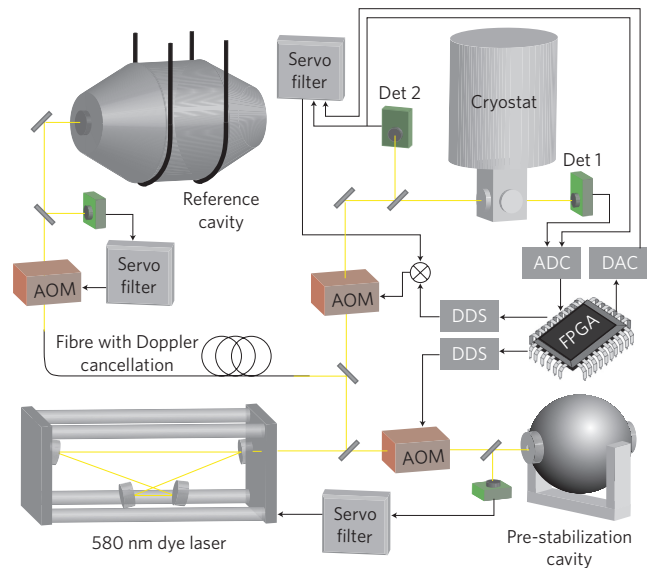

Figure 1 | The $Eu^{3+}:Y_2SiO_5$ spectroscopy and laser stabilization experimental set-up. Spectroscopy is performed with a pre-stabilized 580 nm dye laser that illuminates a $Eu^{3+}:Y_2SiO_5$ crystal housed in an optical flow cryostat. A field-programmable gate array (FPGA) with an embedded microprocessor controls the details of the spectroscopy, including laser frequency, light intensity and pulse durations. The frequencies of spectral holes can be compared against the frequency of the pre-stabilization cavity, or against a reference cavity that typically stabilizes the Al^+ clock laser.

[1]National Institute of Standards and Technology, 325 Broadway Street, Boulder, Colorado 80305, USA, [2]Department of Physics, Atomic Physics, Lund University, Professorsgata 1, 223 63 Lund, Sweden. *e-mail: mthorpe@nist.gov
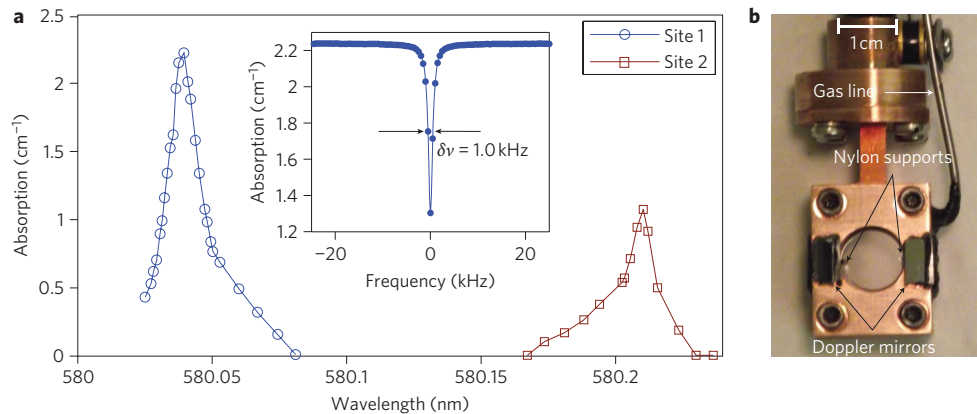
Figure 2 | Eu^{3+}:Y$_2$SiO$_5$ absorption spectrum and crystal housing. a, Absorption spectrum of the $^7F_0 \rightarrow {}^5D_0$ transition in 0.5% doped Eu^{3+}:Y$_2$SiO$_5$ at $T = 4.5$ K. The two inhomogeneously broadened absorption features 'spectral sites 1 and 2' result from the two different positions within the Y$_2$SiO$_5$ unit cell where Eu^{3+} can substitute for Y^{3+}. Inset: single spectral hole written at 580.0390 nm and $T = 4.5$ K with a burn time of 100 ms and a laser intensity of 35 μW cm^{-2}. This hole was measured with 2 ms probe pulses, each separated by 500 Hz (SNR = 1,500). **b**, Image of the sealed chamber that provides a controlled pressure environment and acceleration-insensitive mounting for the Eu^{3+}:Y$_2$SiO$_5$ crystal.

into the Y$_2$SiO$_5$ crystal, the random location of dopants strains the lattice and each ion experiences a slightly different crystal field and corresponding Stark shift[24]. As a result, the Eu^{3+}:Y$_2$SiO$_5$ absorption spectrum is inhomogeneously broadened[25,26]. Spectral holes are 'burned' by laser excitation of those Eu^{3+} ions that are shifted into resonance by the crystal field. Spontaneous decay into other, long-lived, hyperfine ground states redistributes the ground-state population and leads to transparencies or 'spectral holes'. For the present work, we used a doping of 0.5% Eu^{3+}, with an inhomogeneous linewidth of 10 GHz that, in principle, can contain nearly 1×10^8 resolvable spectral holes. At T = 2.0 K, a lifetime of 20 days has been measured[25]. However, the lifetime depends strongly on temperature. For our operating temperature ($T = 4.5$ K), the lifetime exceeds a day, but the spectral holes last only 1 s at 15 K. Therefore, a spectral-hole pattern can be used for long-term laser stabilization at $T \leq 4.5$ K, and can be easily erased if the temperature is increased.

In this Article, we describe a two-stage laser-stabilization system (Fig. 1), in which a FP cavity first stabilizes the laser frequency to $\sigma_y(\tau) \approx 1 \times 10^{-14}$ (0.1 s < τ < 10 s). The pre-stabilized laser is then modulated to address a spectral-hole pattern containing 1×10^{15} atomic absorbers within a 0.4 cm^3 Eu^{3+}:Y$_2$SiO$_5$ crystal, and a servo simultaneously writes and stabilizes the laser to the spectral holes. By using a pre-stabilized laser and many spectral holes, we derive an error signal for laser stabilization while reducing perturbations to the spectral memory. Here we demonstrate the use of 10 to 100 spectral holes to stabilize a 580 nm laser to $\sigma_y(\tau) = 6 \times 10^{-16}$ for 2 s < τ < 8 s. We also report several properties of Eu^{3+}:Y$_2$SiO$_5$ that make this material a promising candidate for achieving higher laser stability than is currently available via optical cavities.

Results

The absorption spectrum for the $^7F_0 \rightarrow {}^5D_0$ transition in 0.5% doped Eu^{3+}:Y$_2$SiO$_5$ at $T = 4.5$ K is shown in Fig. 2a. The two resolved peaks at vacuum wavelengths of 580.0390 nm and 580.2110 nm result from two different locations within the Y$_2$SiO$_5$ crystal unit cell where Eu^{3+} can substitute for Y^{3+}. These features are referred to as spectral sites 1 and 2, respectively. The inset to Fig. 2a shows a single spectral hole with a linewidth of 1.0 kHz, a 40% contrast and an SNR of 1,500, written at 580.0390 nm and $T = 4.5$ K. Although photon-echo measurements suggest that Eu^{3+}:Y$_2$SiO$_5$ spectral holes as narrow as 100 Hz are possible[23], so far we have not observed linewidths narrower than 500 Hz. This broader linewidth is partially due to phonon scattering, which

contributes 300 Hz to the homogeneous linewidth at $T = 4.5$ K (ref. 25). Further broadening may be caused by vibrations or fluctuations in electric or magnetic fields in our cryostat, which could be improved in future systems. We used two protocols for writing and detecting spectral holes. For characterizing the sensitivity to environmental perturbations we wrote the holes at a relatively high intensity (35–140 μW cm^{-2}) for durations of 10–200 ms, and detected the holes at lower intensities (3 μW cm^{-2}) with shorter pulse durations (1 ms). For laser stabilization we wrote and detected the pattern with the low-intensity (3 μW cm^{-2}) and short-duration (1 ms) pulses.

The Eu^{3+}:Y$_2$SiO$_5$ crystal was housed in an optical flow cryostat to provide the ability to vary the crystal temperature continuously from 2.0 K to 300 K (Fig. 1). Inside the cryostat, the crystal was enclosed in a second sealed chamber filled with helium gas, so that the pressure and temperature environment could be controlled independently (Fig. 2b). A gas line led from the sealed chamber to a manifold outside the cryostat where the pressure was controlled and monitored. Figure 3 shows the pressure and temperature sensitivity of the spectral-hole frequency. The pressure sensitivities, $\alpha_1 = -211.4(4)$ Hz Pa^{-1} for site 1 and $\alpha_2 = -52.0(7)$ Hz Pa^{-1} for site 2, are shown in Fig. 3a. By combining the pressure sensitivity with the bulk modulus of Y$_2$SiO$_5$ (135 GPa), we calculate the sensitivity of spectral holes to changes in the volume of the crystal ($\delta f/f = 0.055 \times \delta V/V$ for site 1 and $\delta f/f = 0.014 \times \delta V/V$ for site 2). Compared to FP cavities where $\delta f/f = 0.33 \delta V/V$ and the typical bulk modulus is 34 GPa (ref. 27), spectral holes have significant isolation from mechanical instability that not only makes them less sensitive to accelerations, but also reduces their susceptibility to thermal noise.

Measurements of the temperature sensitivity for sites 1 and 2 are shown in Fig. 3b,c, respectively. The data show the temperature sensitivities κ_i for sites ($i \in \{1, 2\}$) in the absence of a background gas ($P = 0$ Pa). Site 1 displays a lower temperature sensitivity than site 2, and an anomalous backward bending of the curve at 7.5 K. These curves provide a high-resolution extension of data presented by Könz and colleagues[25]. When the sealed chamber is filled with helium gas, the pressure and temperature of the gas are related through the ideal gas law. Furthermore, because the pressure sensitivity has a negative slope, and the temperature sensitivity has a positive slope (for 2.0 K < T < 7.5 K), certain combinations of pressure and temperature lead to a vanishing first-order term of the temperature sensitivity. This effect is illustrated in Fig. 3b,c. Because the gas manifold is outside the cryostat, at room
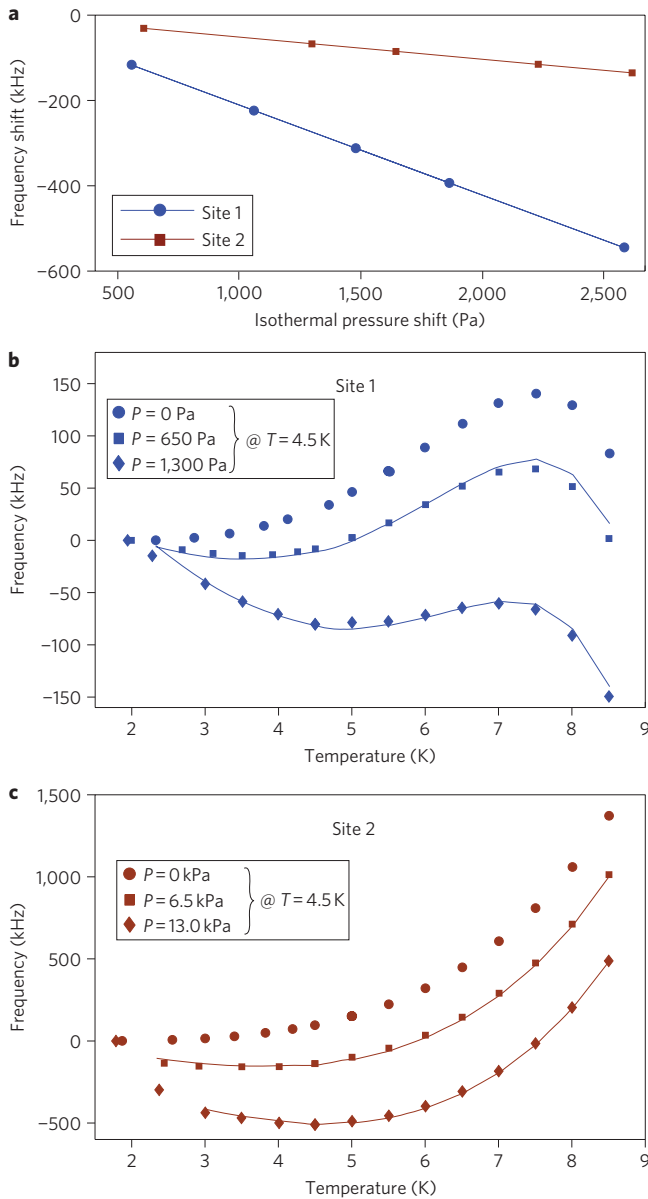
Figure 3 | Pressure and temperature sensitivity of the spectral-hole frequency for spectral sites 1 and 2. a, Pressure sensitivity is $\alpha_1 = -211.4(4)$ Hz Pa^{-1} for holes at site 1 and $\alpha_2 = -52.0(7)$ Hz Pa^{-1} at site 2. **b,c**, Temperature sensitivities for holes at sites 1 and 2 are given by the $P = 0$ Pa data (circles). In a sealed chamber, the gas pressure and temperature are linked by the ideal gas law, and the pressure and temperature sensitivities both contribute to the frequency of the spectral hole. At certain combinations of P and T for each site, the frequency becomes first-order insensitive to the temperature of its environment. The solid lines through the $P \neq 0$ data are expected frequency shifts given the measured pressure and temperature sensitivities and the best-fit volume ratio (see text).

temperature, the gas behaves as a two-reservoir system. The equation of state for this system (see Methods) can be combined with the pressure sensitivity $\alpha_i \Delta P$ and the zero-pressure temperature sensitivity $\kappa_i(T_c)$ functions for each site to determine the spectral-hole temperature sensitivity in the presence of helium gas:

$$f_i(P, T_c) = \kappa_i(T_c) + \alpha_i P(T_c) \qquad (1)$$

Here, f_i is the spectral-hole frequency, $P(T_c)$ is the equation of state and T_c is the temperature of the crystal inside the cryostat. A fit to

the measured data determines the ratio of the cryogenic to room-temperature gas volumes for the current system, $V_c/V_r = 0.022(3)$. This ratio is important, because it determines how strongly temperature and pressure fluctuations in the gas manifold (outside the cryostat) will affect the temperature and pressure of the cryogenic gas volume. The temperature-insensitive points for spectral holes have some advantages over the analogous 'zero-crossing temperature' of the coefficient of thermal expansion for ultralow-expansion glass (ULE) cavities. First, the temperature of the insensitive point for spectral holes can be tuned by changing the pressure of helium gas in the sealed chamber. Second, the spectral holes exhibit reduced temperature sensitivity compared to ULE. For ULE, the quadratic temperature sensitivity is 720 kHz K^{-2} for a cavity operating at 580 nm (ref. 27). The values for Eu^{3+}:Y$_2$SiO$_5$ spectral holes are 16 kHz K^{-2} for site 1 and 114 kHz K^{-2} for site 2. We have measured both the temperature and pressure sensitivity of Eu^{3+}:Y$_2$SiO$_5$ spectral holes for three different crystal samples with two different doping concentrations (0.5% and 0.1%) and have found these results to be consistent for all samples.

A pattern of spectral holes, simultaneously written and used for laser stabilization, is shown in Fig. 4a. For the current experiment, a hole spacing of 50 kHz was chosen to provide a long locking time such that a single hole could grow wider for tens of seconds before coalescing with an adjacent hole. The number of holes (10–100) was chosen to distribute the spectral perturbations due to measurement over many holes and also to extend the locking time. For details about the writing and probing of the spectral-hole pattern, see Methods. During laser stabilization, the pressure and temperature of the crystal environment are held at an insensitive point. At the same time, a Doppler measurement cancels frequency shifts in the spectral-hole pattern due to the motion of the crystal[28]. This measurement is made with a Michelson interferometer where one arm of the interferometer is formed by a mirror attached to the crystal chamber (Fig. 2b). Figure 4b shows the frequency spectrum of the spectral-hole-stabilized laser with and without Doppler cancellation. Two prominent resonances in the crystal motion appear at $f_1 = 14.5$ Hz and $f_2 = 33$ Hz, corresponding to root mean square (r.m.s.) frequency shifts of $\Delta \nu_1 = 12.1$ Hz and $\Delta \nu_2 = 4.3$ Hz, respectively. The 14.5 Hz resonance corresponds to a velocity of $V_{rms} = \Delta \nu_1 c / \nu_o = 7 \times 10^{-6}$ m s^{-1} and an acceleration of $a_{rms} = 2\pi f_1 V_{rms} = 6.4 \times 10^{-4}$ m s^{-2}, where c is the speed of light and $\nu_o = 517$ THz is the laser frequency. When Doppler cancellation is implemented, these shifts are reduced, improving the frequency stability of the hole pattern. The residual frequency shift of $\Delta \nu_{1D} = 0.25$ Hz amplitude (r.m.s.) due to the 14.5 Hz motion provides an estimate of the acceleration sensitivity of the spectral-hole pattern of $\Delta \nu_{1D}/(\nu_o a_{rms}) = 7 \times 10^{-12} g^{-1} (1g = 9.8$ m s^{-2}), which is below the passive acceleration-sensitivity of FP cavities[9,12,29]. As in FP cavities, the acceleration sensitivity depends on the mounting configuration, and further improvements are possible. For the present work, the crystal was supported on two 0.8-mm-thick and 2.5-mm-wide nylon tabs (Fig. 2b). The support points were near the vertical centre of the crystal such that the frequency of spectral holes were nominally insensitive to accelerations[10].

To determine the frequency stability of the spectral-hole laser lock, we independently locked the 580 nm laser to a reference cavity that is typically used to stabilize the clock laser for a ^{27}Al$^+$ optical clock[30]. To ensure that the write/probe laser was locked tightly to the spectral-hole pattern, we injected noise into the pre-stabilization servo, thereby degrading the laser stability to $\sigma_y \approx 1 \times 10^{-14}$. Figure 4c shows the write/probe laser stability and the frequency comparison between the reference cavity and the spectral-hole laser lock with the linear frequency drift subtracted. The reference cavity has a noise floor of $\sigma_y(\tau) \approx 5 \times 10^{-16}$, and a typical drift rate of 0.1 Hz s^{-1}. During the comparison measurements, we observed relative drifts between the spectral-hole
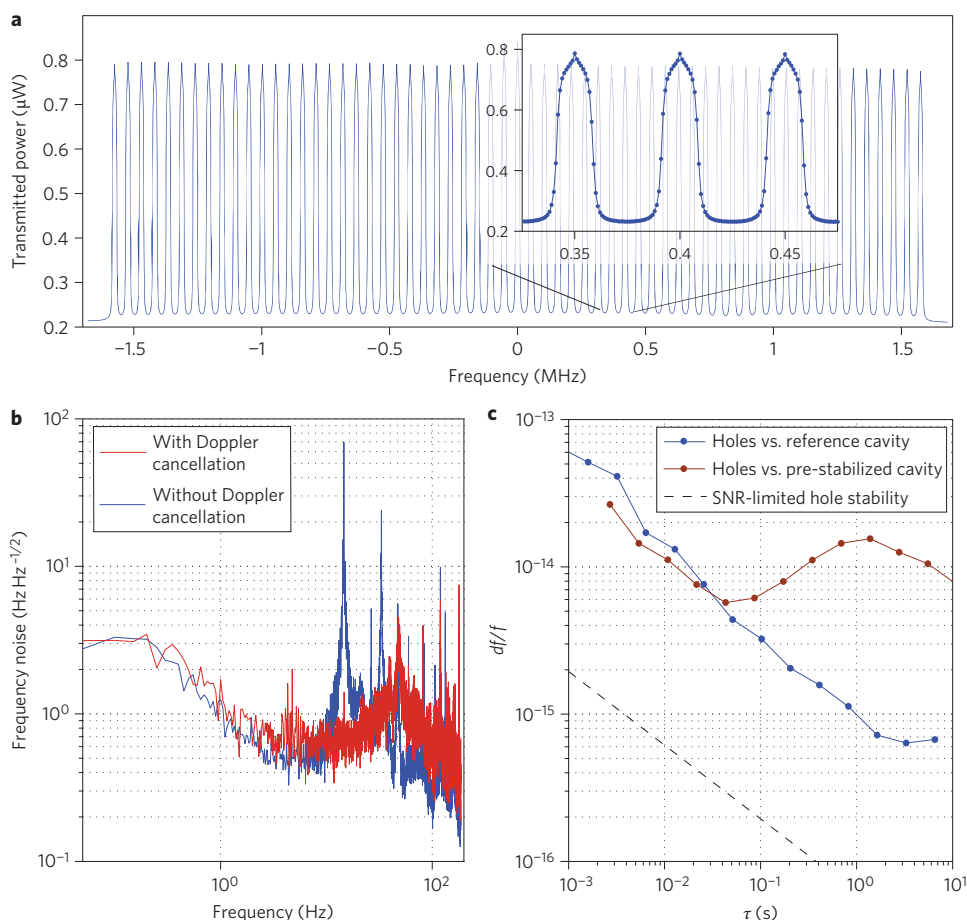
Figure 4 | Laser stabilization to multiple spectral holes. a, A pattern of 61 spectral holes burned at site 1 and spaced by 50 kHz for laser stabilization. The inset shows three of the holes in higher resolution. **b**, Laser frequency noise spectra of the spectral-hole laser lock with and without Doppler cancellation of the crystal motion (30 mHz resolution bandwidth). The motional resonance at 14.5 Hz provides an estimate of the spectral-hole acceleration sensitivity of $7 \times 10^{-12}\ g^{-1}$. **c**, Allan deviation traces of frequency comparisons between the pre-stabilization cavity, the reference cavity and the spectral-hole pattern. The pre-stabilized laser is made artificially noisy, $\sigma_y(\tau) > 1 \times 10^{-14}$ (red trace), and is used to write and lock to a pattern of spectral holes. The spectral-hole lock is then compared to the frequency of a reference cavity that has a noise floor of $\sigma_y(\tau) \approx 5 \times 10^{-16}$ (blue trace, 60 s of data). The black dashed line is the expected short-term stability based on the spectral-hole linewidth and the SNR of the absorption measurements.

pattern and the reference cavity that varied between 0.1 Hz s^{-1} and 0.5 Hz s^{-1}. A noise floor of $\sigma_y = 6.5 \times 10^{-16}$ was observed in the comparison, which is a combination of reference cavity noise and noise from the hole-burning stabilized laser. So far, we have not observed SNR-limited short-term stability of the spectral-hole laser lock (Fig. 4c). We expect that this is due to a combination of pressure fluctuations of the gas reservoir, vibrations in the cryostat, and Dick-effect noise[31] from the write/probe laser due to the 90% duty cycle of our probe pulses. Each of these sources of instability must be addressed to achieve SNR-limited performance.

Discussion

Our initial attempts at laser stabilization have already demonstrated performance that is competitive with the best FP cavities on short timescales. Further improvements are expected by lowering the noise in the detection of light transmitted through the crystal, and the use of two probe beams that enable interleaved measurements of the hole pattern to eliminate Dick-effect noise. In the present configuration, the spectral bandwidth of each 1 ms measurement pulse contains 1×10^{12} absorbers. As a result of the low probe laser intensity, which serves to minimize perturbations to the spectral-hole pattern, photon scattering from roughly 1×10^8 atoms occurs during each measurement. These experimental parameters, including the 15 kHz spectral-hole linewidth shown

in Fig. 4a, correspond to a shot-noise-limited laser stability of $\sigma_y(\tau) = 3.0 \times 10^{-17}/\sqrt{\tau}$.

To achieve a stability of $\sigma_y(\tau) = 3 \times 10^{-17}/\sqrt{\tau}$ will require $\Delta P < 67\ \mu$Pa and $\Delta a < 4\ \mu g$ at averaging time of 1 s, and can be achieved through better engineering of the cryogenic environment. Magnetic field sensitivity measurements indicate that a modest control of the magnetic field $\Delta B < 1 \times 10^{-5}$ T will be required. Finally, owing to the pressure and temperature cancellation at the site 1 insensitive point, an overall temperature stability of $\Delta T < 1.4$ mK is sufficient, but temperature gradients must also be minimized. This technique for achieving low-temperature sensitivity may be useful for other proposed frequency references based on solids such as thorium-doped crystals[32,33].

At longer timescales, frequency comparison measurements are currently limited by the lifetime of the spectral-hole pattern. This limitation needs to be addressed if spectral-hole burning laser stabilization is to become useful for most LLO applications. One approach for dealing with this problem is to write a self-regenerating pattern that eventually achieves a quasi-steady state. This pattern could take the form of a sinusoidal modulation of the absorption spectrum where the population is slowly redistributed by the successive measurements, but the pulse sequence is tailored such that the overall shape of the absorption spectrum remains constant. Such a spectral-hole pattern is possible if the pattern of holes is wide

enough to encompass all of the Eu^{3+} hyperfine ground states, and the hole spacing is small enough that the linewidth of individual absorbers prevents population buildup between adjacent spectral holes. Stabilization to such a steady-state pattern must also compensate for the side-holes and anti-holes that accompany each spectral feature[22].

If the technical sources of frequency noise can be made sufficiently small, the stability of $Eu^{3+}:Y_2SiO_5$ spectral holes will be determined by thermal noise, as in FP cavities. Our measurements of the pressure sensitivity provide some insight into this fundamental limit. If we assume an isotropic crystal geometry and a conservative mechanical loss angle for $Eu^{3+}:Y_2SiO_5$ ($\phi = 1 \times 10^{-3}$), then thermal noise for a crystal of the size used in the present work implies a fractional-frequency instability below 3×10^{-17} (ref. 15). However, many crystalline materials exhibit reduced mechanical loss at cryogenic temperatures, so the mechanical loss angle at 4.5 K may be smaller ($\phi \approx 1 \times 10^{-5}$), leading to a thermal noise floor that is an order of magnitude lower. Nevertheless, Y_2SiO_5 has low crystal symmetry, and a full anisotropic treatment of its thermomechanical properties is required to make accurate estimates of the thermal noise floor[34], as well as to engineer optimal strategies for mounting these crystals to minimize environmental sensitivity.

During the past decade, the frequency stabilities of LLOs based on either FP cavities or spectral-hole burning have improved by 30%, and new optical clocks have a substantial need for further improvements. A combination of the two laser-stabilization approaches has the potential to yield order-of-magnitude stability gains due to the low sensitivity of $Eu^{3+}:Y_2SiO_5$ spectral holes to environmental perturbations and internal noise. Such gains could benefit a wide range of LLO applications, including the realization of atomic time, gravitational measurements for geodesy, radar and communications applications, and very long baseline interferometry.

Methods

The experimental set-up for high-resolution spectroscopy of $Eu^{3+}:Y_2SiO_5$ spectral holes is shown in Fig. 1. The output of a 580 nm dye laser was split into three beamlines that provide pre-stabilization of the laser frequency, frequency comparisons with a reference cavity, and a write/probe beam for $Eu^{3+}:Y_2SiO_5$ spectroscopy. The laser was locked to the pre-stabilization cavity using the PDH scheme. With optimal locking, the laser can achieve a stability of $\sigma_y(\tau) = 1.2 \times 10^{-15}$ (0.5 s $< \tau <$ 12 s)[29]. For spectral-hole laser locking experiments we intentionally reduced the stability of the write/probe laser ($\sigma_y(\tau) > 1 \times 10^{-14}$ for 0.3 s $< \tau <$ 6 s) to clearly demonstrate the stability of the spectral holes. For optimal performance, the pre-stabilization laser must have a linewidth of much less than 1 kHz so that the spectral-hole linewidth is not broadened due to writing with the noisy laser. An acousto-optic modulator (AOM) was placed before the cavity, enabling laser frequency adjustments of the 'reference cavity' and 'write/probe' beam-lines that are independent of the pre-stabilization cavity lock.

For temperatures above 4.2 K, the crystal temperature was controlled by a servo that heats helium vapour surrounding the sealed chamber. For temperatures below 4.2 K, the heater was turned off and a scroll pump and pressure regulator were used to lower the pressure, and hence the temperature, of the helium vapour. In the range from 2.0 K to 10.0 K, the temperature could be controlled to within 1 mK. The sealed chamber was filled with helium gas by a 0.9-mm-inner-diameter tube that extended from the chamber inside the cryostat to the room-temperature gas manifold. A capacitive pressure gauge located on the room-temperature gas manifold was used to monitor the pressure inside the sealed chamber. The pressure and temperature of this system are related by

$$P = \frac{k_B C T_c}{1 + \frac{T_c V_r}{T_r V_c}} \qquad (2)$$

where P is the pressure of the system, k_B is the Boltzmann constant, T_r (T_c) correspond to the room (cryostat) temperature, V_r (V_c) are the room-temperature (cryogenic) gas volumes and C is the total number of helium atoms divided by V_c.

$Eu^{3+}:Y_2SiO_5$ spectroscopy was performed by measuring the frequency-dependent absorption of light transmitted through the $Eu^{3+}:Y_2SiO_5$ crystal. For the current work, the crystal was illuminated by a single 6-mm-diameter beam aligned to propagate through the centre of the crystal sample. The intensity, frequency and duration of the illumination were controlled by a microprocessor embedded in a field-programmable gate array (FPGA). The FPGA instructed a digital-to-analog converter (DAC) to output voltage pulses to an intensity servo to control the optical

power and pulse duration. Before each pulse, the FPGA set the frequency of a direct digital synthesizer (DDS) that drove the broadband AOM located before the cryostat. In the current set-up, the frequency of the incident beam could be tuned over 600 MHz of bandwidth, and the beam intensity could be set to values between $0.1 \, \mu W \, cm^{-2}$ and $200 \, \mu W \, cm^{-2}$. The incident and transmitted beams, detected by 'Det 1' and 'Det 2' and digitized by an analog-to-digital converter (ADC), were used to calculate the absorption for each experiment.

For laser stabilization experiments, the embedded microprocessor controlled the process for simultaneously writing and probing the spectral-hole pattern. Experimental parameters such as the number of holes, hole spacing, centre frequency of the pattern, servo gains, pulse duration and pulse power were adjustable by the user. To generate a spectral-hole pattern, a single hole was first burned with successive pulses until a target hole depth (typically 30% contrast) was reached. Each time a hole reached the target depth, the burning process for a new hole was initiated until the pattern contained the pre-specified number of holes. When holes exceeded the target depth they were deemed ready for laser stabilization. During the burning process there were two categories of holes, those ready for stabilization and those still in the burning process. The servo interleaved burning pulses on unfinished holes with frequency stabilization measurements on sufficiently deep holes until all holes exceeded the target depth. For each frequency measurement and burn operation, a random hole was selected from the corresponding group. This bootstrapping process established the regular pattern of spectral holes seen in Fig. 4a. Owing to the combination of centre burn and measurement pulses, the spectral holes took on a broad, steep-walled, shape with a sharp peak in the centre. The 1 ms duration of each measurement pulse and the 90% measurement duty cycle led to a servo bandwidth of 450 Hz. In this configuration, we experimentally determined that the write/probe laser must have a stability of $\sigma_y(\tau) < 1 \times 10^{-13}$ to achieve optimal performance. However, with a greater feedback bandwidth, it is expected that a noisier pre-stabilized laser could be used.

Frequency stabilization measurements were made by recording the absorption on both sides of a hole at roughly two-thirds of the maximum depth. These measurements were subtracted, multiplied by the servo gain, and fed back to the frequency of the AOM positioned before the pre-stabilization cavity. As the holes were measured continually, they became both deeper and wider. The frequency measurement data were used in a secondary feedback loop to track the width of each hole to ensure that servo measurements were always made at roughly two-thirds of the hole depth. For each frequency measurement, the hole was also burned at the centre frequency until its contrast approached 100% so that each hole retained a single-peaked shape. Once all holes reached full contrast, only frequency measurements were performed and the measurement duty cycle was 90%. Finally, a small amount of gain was used to adjust the laser probe frequency for each hole to remove frequency errors that occurred because the holes were written with a noisy laser.

To determine the stability of the pre-stabilization cavity and spectral-hole pattern laser locks, frequency comparisons were made with a reference cavity. Light from the dye laser was delivered to the reference cavity over a Doppler-noise-cancelled fibre. The laser was locked to the reference cavity with a PDH error signal that was fed back to an AOM positioned before the cavity. When locked, the AOM drive frequency provided a measure of the frequency difference between the reference cavity and the pre-stabilization cavity (if the spectral-hole laser lock was inactive) or the spectral-hole laser lock when active.

References

1. Rosenband, T. *et al.* Frequency ratio of Al^+ and Hg^+ single-ion optical clocks; metrology at the 17th decimal place. *Science* **28,** 1808–1812 (2008).
2. Blatt, S. *et al.* New limits on coupling of fundamental constants to gravity using ^{87}Sr optical lattice clocks. *Phys. Rev. Lett.* **100,** 140801 (2008).
3. Chou, C. W., Hume, D. B., Rosenband, T. & Wineland, D. J. Optical clocks and relativity. *Science* **329,** 1630–1633 (2010).
4. Bartels, A. *et al.* Femtosecond-laser-based synthesis of ultrastable microwave signals from optical frequency references. *Opt. Lett.* **30,** 667–669 (2005).
5. Zhang, W. *et al.* Sub-100 attoseconds stability optics-to-microwave synchronization. *Appl. Phys. Lett.* **96,** 211105 (2010).
6. Fortier, T. M. *et al.* Generation of ultrastable microwaves via optical frequency division. *Nature Photon.* **5,** 425–429 (2011).
7. Drever, R. W. P. *et al.* Laser phase and frequency stabilization using an optical resonator. *Appl. Phys. B* **31,** 97–105 (1983).
8. Young, B. C., Cruz, F. C., Itano, W. M. & Bergquist, J. C. Visible lasers with subhertz linewidths. *Phys. Rev. Lett.* **82,** 3799–3802 (1999).
9. Jiang, Y. Y. *et al.* Making optical atomic clocks more stable with 10^{-16}-level laser stabilization. *Nature Photon.* **5,** 158–161 (2011).
10. Notcutt, M., Ma, L. S., Ye, J. & Hall, J. L. Simple and compact 1-Hz laser system via an improved mounting configuration of a reference cavity. *Opt. Lett.* **30,** 1815–1817 (2005).
11. Nazarova, T., Riehle, F. & Sterr, U. Vibration-insensitive reference cavity for an ultra-narrow-linewidth laser. *Appl. Phys. B* **83,** 531–536 (2006).

12. Webster, S. A., Oxborrow, M. & Gill, P. Vibration insensitive optical cavity. *Phys. Rev. A* **75,** 011801 (2007).
13. Millo, J. *et al.* Ultrastable lasers based on vibration insensitive cavities. *Phys. Rev. A* **79,** 053829 (2009).
14. Thorpe, M. J., Leibrandt, D. R., Fortier, T. M. & Rosenband, T. Measurement and real-time cancellation of vibration-induced phase noise in a cavity-stabilized laser. *Opt. Express.* **18,** 18744–18751 (2010).
15. Numata, K., Kemery, A. & Camp, J. Thermal-noise limit in the frequency stabilization of lasers with rigid cavities. *Phys. Rev. Lett.* **93,** 250602 (2004).
16. Notcutt, M. *et al.* Contribution of thermal noise to frequency stability of rigid optical cavity via hertz-linewidth lasers. *Phys. Rev. A* **73,** 031804 (2006).
17. Sellin, P. B., Strickland, N. M., Carlsten, J. L. & Cone, R. L. Programmable frequency reference for subkilohertz laser stabilization by use of persistent spectral hole burning. *Opt. Lett.* **24,** 1038–1040 (1999).
18. Strickland, N. M., Sellin, P. B., Sun, Y., Carlsten, J. L. & Cone, R. L. Laser frequency stabilization using regenerative spectral hole burning. *Phys. Rev. B* **62,** 1473–1476 (2000).
19. Böttger, T., Pryde, G. J. & Cone, R. L. Programmable laser frequency stabilization at 1523 nm by use of persistent spectral hole burning. *Opt. Lett.* **28,** 200–202 (2003).
20. Julsgaard, B., Walther, A., Kröll, S. & Rippe, L. Understanding laser stabilization using spectral hole burning. *Opt. Express* **15,** 11444–11465 (2007).
21. Shelby, R. M. & Macfarlane, R. M. Measurement of the anomalous nuclear magnetic moment of trivalent europium. *Phys. Rev. Lett.* **47,** 1172–1175 (1981).
22. Yano, R., Mitsunaga, M. & Uesugi, N. Ultralong optical dephasing time in Eu^{3+}:Y_2SiO_5. *Opt. Lett.* **16,** 1884–1886 (1991).
23. Equall, R. W., Sun, Y., Cone, R. L. & Macfarlane, R. M. Ultraslow optical dephasing in Eu^{3+}:Y_2SiO_5. *Phys. Rev. Lett.* **72,** 2179–2182 (1994).
24. Stoneham, A. M. Shapes of inhomogeneously broadened resonance lines in solids. *Rev. Mod. Phys.* **41,** 82–108 (1994).
25. Könz, F. *et al.* Temperature and concentration dependence of optical dephasing, spectral-hole lifetime, and anisotropic absorption in Eu^{3+}:Y_2SiO_5. *Phys. Rev. B* **68,** 085109 (2003).
26. Sellars, M. J., Fraval, E. & Longdell, J. J. Investigation of static electric dipole-dipole coupling induced optical inhomogeneous broadening in Eu^{3+}:Y_2SiO_5. *J. Lumin.* **107,** 150–154 (2004).
27. ULE® Corning Code 7972 Ultra Low Expansion Glass, available at http://www.corning.com/docs/specialtymaterials/pisheets/ulebro91106.pdf.
28. Bergquist, J. C., Itano, W. M. & Wineland, D. J. in *International School of Physics 'Enrico Fermi'* (eds Hänsch, T. W. & Inguscio, M) (North-Holland, 1994).
29. Leibrandt, D. R. *et al.* Spherical reference cavities for frequency stabilization of lasers in non-laboratory environments. *Opt. Express* **19,** 3471–3482 (2011).
30. Chou, C. W., Hume, D. B., Koelemeij, J. C. J., Wineland, D. J. & Rosenband, T. Frequency comparison of two high-accuracy Al^+ optical clocks. *Phys. Rev. Lett.* **104,** 070802 (2010).
31. Dick, G. J. Local oscillator induced instabilities in trapped ion frequency standards. *Proceedings of the Precise Time and Time Interval Meeting* 133–147 (1987).
32. Peik, E. & Tamm, Chr. Nuclear laser spectroscopy of the 3.5 eV transition in Th-229. *Europhys. Lett.* **61,** 181–186 (2003).
33. Rellergert, W. G. *et al.* Constraining the evolution of the fundamental constants with a solid-state optical frequency reference based on the ^{229}Th nucleus. *Phys. Rev. Lett.* **104,** 200802 (2010).
34. Heinert, D. *et al.* Potential mechanical loss mechanisms in bulk materials for future gravitational wave detectors. *J. Phys. Conf. Ser.* **228,** 012032 (2010).

Author contributions

M.J.T., T.R. and L.R. designed the experiments. M.J.T., T.M.F. and M.S.K. performed the experiments. M.J.T. and T.R. conducted the data analysis. M.J.T., T.R., L.R. and M.S.K. wrote the manuscript.

Additional information

The authors declare no competing financial interests. Reprints and permission information is available online at http://www.nature.com/reprints. Correspondence and requests for materials should be addressed to M.J.T.